Draft version October 21, 2015
Preprint typeset using LaTeX style emulateapj v. 01/23/15

MBH-N PAPER

G. A. D. Savorgnan[1] and A. W. Graham[1]
Centre for Astrophysics and Supercomputing, Swinburne University of Technology, Hawthorn, Victoria 3122, Australia.
Draft version October 21, 2015

ABSTRACT

blah blah
Subject headings: keywords

1. INTRODUCTION

The empirical Sérsic (1963, 1968) $R^{1/n}$ model has been demonstrated to provide adequate description of the light distribution of the stellar spheroidal and disk components of galaxies (add REFS), yet its physical origin has remained unexplained for decades. The Sérsic model parametrizes the intensity I as a function of the projected galactic radius R such that

$$I(R; I_{\rm e}, R_{\rm e}, n) = I_{\rm e} \exp\left\{-b_{\rm n}\left[\left(\frac{R}{R_{\rm e}}\right)^{1/n} - 1\right]\right\}, \quad (1)$$

where $I_{\rm e}$ indicates the intensity at the effective radius $R_{\rm e}$ that encloses half of the total light from the model, the Sérsic index n is the parameter that regulates the curvature of the radial light profile, and $b_{\rm n}$ is a constant defined in terms of the Sérsic index n (see Graham & Driver 2005, and references therein). A large Sérsic index corresponds to a steep inner profile and a shallow outer profile, whereas a small Sérsic index corresponds to a shallow inner profile and a steep outer profile. This means that, for a stellar spheroidal system whose light distribution is well approximated by the Sérsic model, the larger the Sérsic index is, the more centrally concentrated the stars are and the more extended the outer envelope is.

A compelling physical interpretation for the Sérsic profile family was recently theorized by Cen (2014) and later confirmed by Nipoti (2015) by means of N-body simulations. Cen (2014) conjectured that, when structures form within a standard cold dark matter model seeded by random Gaussian fluctuations, any centrally concentrated stellar structure always possesses an extended stellar envelope, and vice versa. Nipoti (2015) quantitatively explored Cen's hypothesis and showed that systems originated from several mergers have a large Sérsic index ($n \gtrsim 4$), whereas systems with a Sérsic index as small as $n \simeq 2$ can be produced by coherent dissipationless collapse, and exponential profiles ($n = 1$) can only be obtained through dissipative processes. This scenario sets the theoretical framework for the well known correlation between the spheroid luminosity, $L_{\rm sph}$, and the spheroid Sérsic index, $n_{\rm sph}$, (e.g. Young & Currie 1994; Jerjen et al. 2000; Graham & Guzmán 2003), although the numerical results of Nipoti (2015) seem to lack of spheroidal systems with Sérsic indices as large as $7-10$, which are commonly observed in the local Universe.

Given the existence of the $L_{\rm sph} - n_{\rm sph}$ correlation and the relation between the central black hole mass, $M_{\rm BH}$, and the spheroid luminosity (e.g. Magorrian et al. 1998), an $M_{\rm BH} - n_{\rm sph}$ relation must exist. After Graham et al. (2001) showed that the black hole mass is tightly linked to the stellar light concentration of spheroids (measured through a parameter different from, but closely related to the Sérsic index), Graham & Driver (2007) presented for the first time the $M_{\rm BH} - n_{\rm sph}$ correlation using a sample of 27 elliptical and disk galaxies. Graham & Driver (2007) fit their data with a log-quadratic regression, finding that the $M_{\rm BH} - n_{\rm sph}$ log-relation is steeper for spheroids with small Sérsic indices and shallower for spheroids with large Sérsic indices, and measured a relatively small level of scatter[1]. A few years later, Sani et al. (2011), Vika et al. (2012) and Beifiori et al. (2012) performed multi-component decompositions for samples of galaxies similar to that used by Graham & Driver (2007), but they surprisingly failed to recover a strong $M_{\rm BH}-n_{\rm sph}$ relation. This issue was tackled by Savorgnan et al. (2013), who collected the Sérsic index measurements published by Graham & Driver (2007), Sani et al. (2011), Vika et al. (2012) and Beifiori et al. (2012) for a sample of 54 galaxies, and showed that, by rejecting the most discrepant measurements and averaging the remaning ones, a strong $M_{\rm BH}-n_{\rm sph}$ relation was retrieved. Remarkably, Savorgnan et al. (2013) repeated their analysis upon excluding the Sérsic index measurements of Graham & Driver (2007) and still regained a significant $M_{\rm BH} - n_{\rm sph}$ relation. This was suggestive that the individual galaxy decompositions of Sani et al. (2011), Vika et al. (2012) and Beifiori et al. (2012) were not accurate, i.e. each individual study obtained "noisy" Sérsic index measurements which prevented the recovery of a strong $M_{\rm BH} - n_{\rm sph}$ relation.

Motivated by the need of more accurate galaxy decompositions to refine and re-investigate scaling relations between the black hole mass and several galaxy structural parameters, we performed state-of-the-art modelling for the largest sample of galaxies to date (Savorgnan & Graham 2015, hereafter *Paper I*), for which a dynamical measurement of the black hole mass was available. In doing so, we used 3.6 μm *Spitzer* satellite imagery, given its superb capability to trace the stellar mass (Sheth et al. 2010, and references therein). In Savorgnan et al. (2015, hereafter *Paper II*) we examined the correlations between black hole mass and galaxy luminosity,

gsavorgn@astro.swin.edu.au

[1] At the time, the $M_{\rm BH} - \sigma$ relation (Ferrarese & Merritt 2000; Gebhardt et al. 2000) was reported to have the same level of scatter as the $M_{\rm BH} - n_{\rm sph}$ relation ($\simeq 0.3$ dex).

spheroid luminosity and spheroid stellar mass. In this Paper (*Paper III*) we focus on the $M_{\rm BH} - n_{\rm sph}$ relation. This paper is structured as follows...

2. DATA

We populated the $M_{\rm BH} - n_{\rm sph}$ diagram with the same galaxy sample used in *Paper II*, i.e. 66 galaxies for which a dynamical measurement of the black hole mass has been reported in the literature (by Graham & Scott 2013 or Rusli et al. 2013) and for which we were able to successfully model the light distribution and measure the spheroid structural parameters using 3.6 μm *Spitzer* satellite images. Our galaxy decompositions take into account bulge, disks, spiral arms, bars, rings, halo, extended or unresolved nuclear source and partially depleted core, and – for the first time – they were checked to be consistent with the galaxy kinematics (Emsellem et al. 2011; Scott et al. 2014; Arnold et al. 2014). Kinematical information was used to confirm the presence of disk components in the majority of early-type (elliptical + lenticular) galaxies and, more importantly, to estabilish the radial extent of these disks. This enabled us to distinguish between intermediate-scale disks, that are fully embedded in the spheroid, and large-scale disks, that encase the bulge and dominate the light at large radii (see Savorgnan & Graham 2015 for a discussion on this topic).

Spheroid magnitudes were derived from our state-ofthe- art galaxy decompositions, which take into account bulge, disks, spiral arms, bars, rings, halo, extended or unresolved nuclear source and partially depleted core. Kinematical information (Emsellem et al. 2011; Scott et al. 2014; Arnold et al. 2014) was used to con

rm the presence of rotationally supported disk components in most early-type (elliptical + lenticular) galaxies, and to identify their extent (intermediate-scale disks that are fully embedded in the bulge, or large-scale disks that encase the bulge and dominate the light at large radii). It is worth stressing that, contrary to common knowledge, the majority of elliptical galaxies contain disks, i.e. they are not single-component spheroidal systems. Paper I presents the dataset used here, including details about the data reduction process and the galaxy modelling technique that we developed. It also discusses how we estimated the uncertainties5 on the bulge magnitudes, along with a comparison and discussion of past decompositions. elliptical/lenticular; S0 = lenticular; S0/Sp = lenticular/ spiral; Sp = spiral; and merger") follows from the galaxy models presented in Paper I. Throughout this paper we will refer to early-type galaxies (E+S0) and latetype galaxies (Sp). Two galaxies classi

ed as E/S0 are obviously included in the early-type bin, whereas two galaxies classi

ed as S0/Sp and another two classi

ed as mergers are included in neither the early- nor the latetype bin.

3. RESULTS

kkkkk

REFERENCES

Arnold, J. A., Romanowsky, A. J., Brodie, J. P., et al. 2014, ApJ, 791, 80
Beifiori, A., Courteau, S., Corsini, E. M., & Zhu, Y. 2012, MNRAS, 419, 2497
Cen, R. 2014, ApJ, 790, L24
Emsellem, E., Cappellari, M., Krajnović, D., et al. 2011, MNRAS, 414, 888
Ferrarese, L., & Merritt, D. 2000, ApJ, 539, L9
Gebhardt, K., Bender, R., Bower, G., et al. 2000, ApJ, 539, L13
Graham, A. W., & Driver, S. P. 2005, PASA, 22, 118
—. 2007, ApJ, 655, 77
Graham, A. W., Erwin, P., Caon, N., & Trujillo, I. 2001, ApJ, 563, L11
Graham, A. W., & Guzmán, R. 2003, AJ, 125, 2936
Graham, A. W., & Scott, N. 2013, ApJ, 764, 151
Jerjen, H., Binggeli, B., & Freeman, K. C. 2000, AJ, 119, 593
Magorrian, J., Tremaine, S., Richstone, D., et al. 1998, AJ, 115, 2285
Nipoti, C. 2015, ApJ, 805, L16
Rusli, S. P., Erwin, P., Saglia, R. P., et al. 2013, AJ, 146, 160
Sani, E., Marconi, A., Hunt, L. K., & Risaliti, G. 2011, MNRAS, 413, 1479
Savorgnan, G., Graham, A. W., Marconi, A., et al. 2013, MNRAS, 434, 387
Scott, N., Davies, R. L., Houghton, R. C. W., et al. 2014, MNRAS, 441, 274
Sérsic, J. L. 1963, Boletin de la Asociacion Argentina de Astronomia La Plata Argentina, 6, 41
—. 1968, Atlas de galaxias australes
Sheth, K., Regan, M., Hinz, J. L., et al. 2010, PASP, 122, 1397
Vika, M., Driver, S. P., Cameron, E., Kelvin, L., & Robotham, A. 2012, MNRAS, 419, 2264
Young, C. K., & Currie, M. J. 1994, MNRAS, 268, L11

TABLE 1
GALAXY SAMPLE.

Galaxy	**Type**	**Distance** [Mpc]	$M_{\mathbf{BH}}$ [10^8 $M_\odot$]	$MAG_{\mathbf{sph}}$ [mag]	$n_{\mathbf{sph}}$
(1)	(2)	(3)	(4)	(5)	(6)
IC 1459	E	28.4	24^{+10}_{-10}	$-26.15^{+0.18}_{-0.11}$	$6.6^{+0.9}_{-0.8}$
IC 2560	Sp (bar)	40.7	$0.044^{+0.044}_{-0.022}$	$-22.27^{+0.66}_{-0.58}$	$0.8^{+0.4}_{-0.3}$
IC 4296	E	40.7	11^{+2}_{-2}	$-26.35^{+0.18}_{-0.11}$	$5.8^{+0.8}_{-0.7}$
M104	S0/Sp	9.5	$6.4^{+0.4}_{-0.4}$	$-23.91^{+0.66}_{-0.58}$	$5.8^{+2.7}_{-1.8}$
M105	E	10.3	4^{+1}_{-1}	$-24.29^{+0.66}_{-0.58}$	$5.2^{+2.4}_{-1.6}$
M106	Sp (bar)	7.2	$0.39^{+0.01}_{-0.01}$	$-21.11^{+0.18}_{-0.11}$	$2.0^{+0.3}_{-0.2}$
M31	Sp (bar)	0.7	$1.4^{+0.9}_{-0.3}$	$-22.74^{+0.18}_{-0.11}$	$2.2^{+0.3}_{-0.3}$
M49	E	17.1	25^{+3}_{-1}	$-26.54^{+0.18}_{-0.11}$	$6.6^{+0.9}_{-0.8}$
M59	E	17.8	$3.9^{+0.4}_{-0.4}$	$-25.18^{+0.18}_{-0.11}$	$5.5^{+0.8}_{-0.7}$
M64	Sp	7.3	$0.016^{+0.004}_{-0.004}$	$-21.54^{+0.18}_{-0.11}$	$0.8^{+0.1}_{-0.1}$
M81	Sp (bar)	3.8	$0.74^{+0.21}_{-0.11}$	$-23.01^{+0.88}_{-0.66}$	$1.7^{+1.3}_{-0.7}$
M84	E	17.9	$9.0^{+0.9}_{-0.8}$	$-26.01^{+0.66}_{-0.58}$	$7.8^{+3.6}_{-2.5}$
M87	E	15.6	$58.0^{+3.5}_{-3.5}$	$-26.00^{+0.66}_{-0.58}$	$10.0^{+4.7}_{-3.2}$
M89	E	14.9	$4.7^{+0.5}_{-0.5}$	$-24.48^{+0.66}_{-0.58}$	$4.6^{+2.2}_{-1.5}$
M94	Sp (bar)	4.4	$0.060^{+0.014}_{-0.014}$	$-22.08^{+0.18}_{-0.11}$	$0.9^{+0.1}_{-0.1}$
M96	Sp (bar)	10.1	$0.073^{+0.015}_{-0.015}$	$-22.15^{+0.18}_{-0.11}$	$1.5^{+0.2}_{-0.2}$
NGC 0524	S0	23.3	$8.3^{+2.7}_{-1.3}$	$-23.19^{+0.18}_{-0.11}$	$1.1^{+0.2}_{-0.1}$
NGC 0821	E	23.4	$0.39^{+0.26}_{-0.09}$	$-24.00^{+0.88}_{-0.66}$	$5.3^{+4.1}_{-2.3}$
NGC 1023	S0 (bar)	11.1	$0.42^{+0.04}_{-0.04}$	$-22.82^{+0.18}_{-0.11}$	$2.1^{+0.3}_{-0.3}$
NGC 1300	Sp (bar)	20.7	$0.73^{+0.69}_{-0.35}$	$-22.06^{+0.66}_{-0.58}$	$3.8^{+1.8}_{-1.2}$
NGC 1316	merger	18.6	$1.50^{+0.75}_{-0.80}$	$-24.89^{+0.66}_{-0.58}$	$2.0^{+1.0}_{-0.7}$
NGC 1332	E/S0	22.3	14^{+2}_{-2}	$-24.89^{+0.88}_{-0.66}$	$5.1^{+3.9}_{-2.2}$
NGC 1374	E	19.2	$5.8^{+0.5}_{-0.5}$	$-23.68^{+0.18}_{-0.11}$	$3.7^{+0.5}_{-0.5}$
NGC 1399	E	19.4	$4.7^{+0.6}_{-0.6}$	$-26.43^{+0.18}_{-0.11}$	$10.0^{+1.4}_{-1.2}$
NGC 2273	Sp (bar)	28.5	$0.083^{+0.004}_{-0.004}$	$-23.00^{+0.66}_{-0.58}$	$2.1^{+1.0}_{-0.7}$
NGC 2549	S0 (bar)	12.3	$0.14^{+0.02}_{-0.13}$	$-21.25^{+0.18}_{-0.11}$	$2.3^{+0.3}_{-0.3}$
NGC 2778	S0 (bar)	22.3	$0.15^{+0.09}_{-0.10}$	$-20.80^{+0.66}_{-0.58}$	$1.3^{+0.6}_{-0.4}$
NGC 2787	S0 (bar)	7.3	$0.40^{+0.04}_{-0.05}$	$-20.11^{+0.66}_{-0.58}$	$1.1^{+0.5}_{-0.4}$
NGC 2974	Sp (bar)	20.9	$1.7^{+0.2}_{-0.2}$	$-22.95^{+0.66}_{-0.58}$	$1.4^{+0.7}_{-0.5}$
NGC 3079	Sp (bar)	20.7	$0.024^{+0.024}_{-0.012}$	$-23.01^{+0.66}_{-0.58}$	$1.3^{+0.6}_{-0.4}$
NGC 3091	E	51.2	36^{+1}_{-2}	$-26.28^{+0.18}_{-0.11}$	$7.6^{+1.0}_{-0.9}$
NGC 3115	E/S0	9.4	$8.8^{+10.0}_{-2.7}$	$-24.22^{+0.18}_{-0.11}$	$4.4^{+0.6}_{-0.5}$
NGC 3227	Sp (bar)	20.3	$0.14^{+0.10}_{-0.06}$	$-21.76^{+0.66}_{-0.58}$	$1.7^{+0.8}_{-0.5}$
NGC 3245	S0 (bar)	20.3	$2.0^{+0.5}_{-0.5}$	$-22.43^{+0.18}_{-0.11}$	$2.9^{+0.4}_{-0.3}$
NGC 3377	E	10.9	$0.77^{+0.04}_{-0.06}$	$-23.49^{+0.66}_{-0.58}$	$7.7^{+3.6}_{-2.5}$
NGC 3384	S0 (bar)	11.3	$0.17^{+0.01}_{-0.02}$	$-22.43^{+0.18}_{-0.11}$	$1.6^{+0.2}_{-0.2}$
NGC 3393	Sp (bar)	55.2	$0.34^{+0.02}_{-0.02}$	$-23.48^{+0.66}_{-0.58}$	$3.4^{+1.6}_{-1.1}$
NGC 3414	E	24.5	$2.4^{+0.3}_{-0.3}$	$-24.35^{+0.18}_{-0.11}$	$4.8^{+0.7}_{-0.6}$
NGC 3489	S0/Sp (bar)	11.7	$0.058^{+0.008}_{-0.008}$	$-21.13^{+0.66}_{-0.58}$	$1.5^{+0.7}_{-0.5}$
NGC 3585	E	19.5	$3.1^{+1.4}_{-0.6}$	$-25.52^{+0.66}_{-0.58}$	$5.2^{+2.4}_{-1.7}$
NGC 3607	E	22.2	$1.3^{+0.5}_{-0.5}$	$-25.36^{+0.66}_{-0.58}$	$5.5^{+2.6}_{-1.7}$
NGC 3608	E	22.3	$2.0^{+1.1}_{-0.6}$	$-24.50^{+0.66}_{-0.58}$	$5.2^{+2.4}_{-1.7}$
NGC 3842	E	98.4	97^{+30}_{-26}	$-27.00^{+0.18}_{-0.11}$	$8.1^{+1.1}_{-1.0}$
NGC 3998	S0 (bar)	13.7	$8.1^{+2.0}_{-1.9}$	$-22.32^{+0.88}_{-0.66}$	$1.2^{+0.9}_{-0.5}$
NGC 4026	S0 (bar)	13.2	$1.8^{+0.6}_{-0.3}$	$-21.58^{+0.88}_{-0.66}$	$2.4^{+1.8}_{-1.0}$
NGC 4151	Sp (bar)	20.0	$0.65^{+0.07}_{-0.07}$	$-23.40^{+0.66}_{-0.58}$	$1.4^{+0.6}_{-0.4}$
NGC 4261	E	30.8	5^{+1}_{-1}	$-25.72^{+0.66}_{-0.58}$	$4.7^{+2.2}_{-1.5}$
NGC 4291	E	25.5	$3.3^{+0.9}_{-2.5}$	$-24.05^{+0.66}_{-0.58}$	$4.2^{+2.0}_{-1.4}$
NGC 4388	Sp (bar)	17.0	$0.075^{+0.002}_{-0.002}$	$-21.26^{+0.88}_{-0.66}$	$0.6^{+0.5}_{-0.3}$
NGC 4459	S0	15.7	$0.68^{+0.13}_{-0.13}$	$-23.48^{+0.66}_{-0.58}$	$3.1^{+1.5}_{-1.0}$
NGC 4473	E	15.3	$1.2^{+0.4}_{-0.9}$	$-23.88^{+0.66}_{-0.58}$	$2.3^{+1.1}_{-0.7}$
NGC 4564	S0	14.6	$0.60^{+0.03}_{-0.09}$	$-22.30^{+0.18}_{-0.11}$	$2.6^{+0.4}_{-0.3}$
NGC 4596	S0 (bar)	17.0	$0.79^{+0.38}_{-0.33}$	$-22.73^{+0.18}_{-0.11}$	$2.7^{+0.4}_{-0.3}$

Galaxy	**Type**	**Distance**	$M_{\rm BH}$	$MAG_{\rm sph}$	$n_{\rm sph}$
		[Mpc]	[10^8 $M_\odot$]	[mag]	
(1)	(2)	(3)	(4)	(5)	(6)
NGC 4697	E	11.4	$1.8^{+0.2}_{-0.1}$	$-24.82^{+0.88}_{-0.66}$	$7.2^{+5.5}_{-3.1}$
NGC 4889	E	103.2	210^{+160}_{-160}	$-27.54^{+0.18}_{-0.11}$	$8.1^{+1.1}_{-1.0}$
NGC 4945	Sp (bar)	3.8	$0.014^{+0.014}_{-0.007}$	$-20.96^{+0.66}_{-0.58}$	$1.4^{+0.7}_{-0.5}$
NGC 5077	E	41.2	$7.4^{+4.7}_{-3.0}$	$-25.45^{+0.18}_{-0.11}$	$4.2^{+0.6}_{-0.5}$
NGC 5128	merger	3.8	$0.45^{+0.17}_{-0.10}$	$-23.89^{+0.88}_{-0.66}$	$1.2^{+0.9}_{-0.5}$
NGC 5576	E	24.8	$1.6^{+0.3}_{-0.4}$	$-24.44^{+0.18}_{-0.11}$	$3.3^{+0.5}_{-0.4}$
NGC 5845	S0	25.2	$2.6^{+0.4}_{-1.5}$	$-22.96^{+0.88}_{-0.66}$	$2.5^{+1.9}_{-1.1}$
NGC 5846	E	24.2	11^{+1}_{-1}	$-25.81^{+0.66}_{-0.58}$	$6.4^{+3.0}_{-2.1}$
NGC 6251	E	104.6	5^{+2}_{-2}	$-26.75^{+0.18}_{-0.11}$	$6.8^{+0.9}_{-0.8}$
NGC 7052	E	66.4	$3.7^{+2.6}_{-1.5}$	$-26.32^{+0.18}_{-0.11}$	$4.2^{+0.6}_{-0.5}$
NGC 7619	E	51.5	25^{+8}_{-3}	$-26.35^{+0.66}_{-0.58}$	$5.3^{+2.5}_{-1.7}$
NGC 7768	E	112.8	13^{+5}_{-4}	$-26.90^{+0.66}_{-0.58}$	$8.4^{+3.9}_{-2.7}$
UGC 03789	Sp (bar)	48.4	$0.108^{+0.005}_{-0.005}$	$-22.77^{+0.88}_{-0.66}$	$1.9^{+1.4}_{-0.8}$

NOTE. — *Column (1)*: Galaxy name. *Column (2)*: Morphological type (E=elliptical, S0=lenticular, Sp=spiral, merger). The morphological classification of four galaxies is uncertain (E/S0 or S0/Sp). The presence of a bar is indicated. *Column (3)*: Distance. *Column (4)*: Black hole mass. *Column (5)*: Absolute 3.6 μm spheroid magnitude. *Column (6)*: Spheroid major-axis Sérsic index. Spheroid magnitudes and Sérsic indices come from our state-of-the-art multicomponent galaxy decompositions (*Paper I*), which include bulges, disks, bars, spiral arms, rings, haloes, extended or unresolved nuclear sources and partially depleted cores, and that – for the first time – were checked to be consistent with the galaxy kinematics. The uncertainties were estimated with a method that takes into account systematic errors, which are typically not considered by popular 2D fitting codes.

TABLE 2
LINEAR REGRESSION ANALYSIS OF THE $L_{\rm sph} - n_{\rm sph}$ DIAGRAM.

Subsample (size)	**Regression**	$\boldsymbol{\alpha}$	$\boldsymbol{\beta}$	$\langle \log n_{\rm sph} \rangle$	$\boldsymbol{\epsilon}$	$\boldsymbol{\Delta}$
	$MAG_{\rm sph}/[\rm mag] = \alpha + \beta\big(\log n_{\rm sph} - \langle \log n_{\rm sph,maj} \rangle\big)$					
All (62)	BCES $(Y\|X)$	-23.88 ± 0.15	-7.17 ± 0.80	0.51	–	1.18
	mFITEXY $(Y\|X)$	-23.95 ± 0.13	-6.70 ± 0.45	0.51	$0.56^{+0.15}_{-0.10}$	0.98
	`linmix_err` $(Y\|X)$	-23.92 ± 0.15	-6.40 ± 0.57	0.51	0.74 ± 0.13	1.07
	BCES $(X\|Y)$	-23.88 ± 0.14	-6.70 ± 0.51	0.51	–	1.11
	mFITEXY $(X\|Y)$	-23.94 ± 0.14	-7.50 ± 0.52	0.51	$0.59^{+0.17}_{-0.11}$	1.23
	`linmix_err` $(X\|Y)$	-23.94 ± 0.16	-7.51 ± 0.62	0.51	0.81 ± 0.16	1.23
	BCES Bisector	-23.88 ± 0.14	-6.93 ± 0.60	0.51	–	1.14
	mFITEXY Bisector	-23.94 ± 0.13	-7.08 ± 0.34	0.51	–	1.16
	`linmix_err` Bisector	-23.93 ± 0.16	-6.91 ± 0.42	0.51	–	1.14
Elliptical (30)	BCES $(Y\|X)$	-25.46 ± 1.12	38.47 ± 114.45	0.76	–	6.37
	mFITEXY $(Y\|X)$	-25.74 ± 0.18	-9.74 ± 1.59	0.76	$0.24^{+0.32}_{-0.24}$	0.94
	`linmix_err` $(Y\|X)$	-25.65 ± 0.21	-7.87 ± 2.15	0.76	0.61 ± 0.22	1.06
	BCES $(X\|Y)$	-25.46 ± 0.23	-10.73 ± 3.21	0.76	–	1.29
	mFITEXY $(X\|Y)$	-25.74 ± 0.20	-10.42 ± 1.79	0.76	$0.22^{+0.38}_{-0.22}$	1.29
	`linmix_err` $(X\|Y)$	-25.72 ± 0.28	-10.92 ± 2.70	0.76	0.73 ± 0.34	1.33
	BCES Bisector	-25.46 ± 0.20	0.03 ± 0.05	0.76	–	1.14
	mFITEXY Bisector	-25.74 ± 0.19	-10.07 ± 1.19	0.76	–	1.26
	`linmix_err` Bisector	-25.68 ± 0.25	-9.15 ± 1.74	0.76	–	1.16
Lenticular (11)	BCES $(Y\|X)$	-22.08 ± 1.66	33.52 ± 98.87	0.33	–	6.09
	mFITEXY $(Y\|X)$	-22.11 ± 0.24	-6.31 ± 2.45	0.33	$0.42^{+0.28}_{-0.17}$	0.71
	`linmix_err` $(Y\|X)$			0.33		
	BCES $(X\|Y)$	-22.08 ± 0.19	-6.83 ± 1.16	0.33	–	0.71
	mFITEXY $(X\|Y)$	-21.94 ± 0.44	-13.16 ± 7.91	0.33	$0.61^{+0.60}_{-0.56}$	1.39
	`linmix_err` $(X\|Y)$			0.33		
	BCES Bisector	-22.08 ± 0.30	0.06 ± 0.05	0.33	–	1.09
	mFITEXY Bisector	-22.05 ± 0.35	-8.55 ± 2.79	0.33	–	0.84
	`linmix_err` Bisector			0.33	–	
Spiral (17)	BCES $(Y\|X)$	-22.33 ± 0.26	-5.31 ± 5.83	0.18	–	1.15
	mFITEXY $(Y\|X)$	-22.22 ± 0.19	-2.17 ± 0.98	0.18	$0.53^{+0.24}_{-0.13}$	0.72
	`linmix_err` $(Y\|X)$	-22.26 ± 0.24	-1.53 ± 1.88	0.18	0.71 ± 0.22	0.78
	BCES $(X\|Y)$	-22.33 ± 0.26	-5.19 ± 3.77	0.18	–	1.13
	mFITEXY $(X\|Y)$	-22.28 ± 0.44	-9.08 ± 5.31	0.51	$1.12^{+0.54}_{-0.31}$	1.83
	`linmix_err` $(X\|Y)$	-22.24 ± 0.71	-11.12 ± 13.59	0.18	1.95 ± 2.47	2.24
	BCES Bisector	-22.33 ± 0.26	-5.25 ± 3.38	0.18	–	1.14
	mFITEXY Bisector	-22.23 ± 0.33	-3.60 ± 1.29	0.18	–	0.92
	`linmix_err` Bisector	-22.25 ± 0.53	-2.88 ± 2.66	0.18	–	0.84

TABLE 3
LINEAR REGRESSION ANALYSIS OF THE $L_{\rm sph} - n_{\rm sph}$ DIAGRAM.

Subsample (size)	**Regression**	$\boldsymbol{\alpha}$	$\boldsymbol{\beta}$	$\langle \log n_{\rm sph} \rangle$	$\boldsymbol{\epsilon}$	$\boldsymbol{\Delta}$
Early-type (43)	BCES $(Y\|X)$	-24.55 ± 0.22	-11.84 ± 2.29	0.64	–	1.50
	mFITEXY $(Y\|X)$	-24.74 ± 0.14	-8.86 ± 0.66	0.51	$0.27^{+0.20}_{-0.27}$	0.87
	`linmix_err` $(Y\|X)$	-24.70 ± 0.17	-8.28 ± 0.87	0.64	0.58 ± 0.17	0.98
	BCES $(X\|Y)$	-24.55 ± 0.14	-8.25 ± 0.63	0.64	–	0.96
	mFITEXY $(X\|Y)$	-24.74 ± 0.14	-9.13 ± 0.68	0.64	$0.23^{+0.25}_{-0.23}$	1.08
	`linmix_err` $(X\|Y)$	-24.73 ± 0.18	-9.08 ± 0.87	0.64	0.60 ± 0.21	1.07
	BCES Bisector	-24.55 ± 0.17	-9.73 ± 1.05	0.64	–	1.14
	mFITEXY Bisector	-24.74 ± 0.14	-8.99 ± 0.48	0.64	–	1.06
	`linmix_err` Bisector	-24.72 ± 0.17	-8.66 ± 0.63	0.64	–	1.02
Bulge (30)	BCES $(Y\|X)$	-22.25 ± 0.20	-5.88 ± 3.06	0.26	–	1.16
	mFITEXY $(Y\|X)$	-22.19 ± 0.14	-2.99 ± 0.73	0.26	$0.52^{+0.18}_{-0.10}$	0.75
	`linmix_err` $(Y\|X)$	-22.20 ± 0.17	-2.48 ± 1.21	0.26	0.67 ± 0.15	0.83
	BCES $(X\|Y)$	-22.25 ± 0.20	-5.85 ± 1.83	0.26	–	1.15
	mFITEXY $(X\|Y)$	-22.17 ± 0.25	-7.65 ± 2.43	0.26	$0.87^{+0.30}_{-0.18}$	1.46
	`linmix_err` $(X\|Y)$	-22.16 ± 0.31	-7.80 ± 3.89	0.26	1.18 ± 0.65	1.48
	BCES Bisector	-22.25 ± 0.20	-5.87 ± 2.06	0.26	–	1.16
	mFITEXY Bisector	-22.18 ± 0.20	-4.34 ± 0.84	0.26	–	0.96
	`linmix_err` Bisector	-22.19 ± 0.25	-3.83 ± 1.39	0.26	–	0.91

NOTE. — For each subsample, we indicate $\langle \log n_{\rm sph} \rangle$, its average value of spheroid Sérsic index. In the last two columns, we report ϵ, the intrinsic scatter, and Δ, the total rms scatter in the $L_{\rm sph}$ direction. all - mergers - outliers Both the early- and late-type subsamples do not contain the two galaxies classified as S0/Sp and the two galaxies classified as mergers (45+17=66-2-2).

TABLE 4
LINEAR REGRESSION ANALYSIS OF THE $M_{\rm BH} - n_{\rm sph}$ DIAGRAM.

Subsample (size)	**Regression**	$\boldsymbol{\alpha}$	$\boldsymbol{\beta}$	$\langle \log n_{\rm sph} \rangle$	$\boldsymbol{\epsilon}$	$\boldsymbol{\Delta}$
	$\log(M_{\rm BH}/[{\rm M}_\odot]) = \alpha + \beta(\log n_{\rm sph} - \langle \log n_{\rm sph} \rangle)$					
All (62)	BCES $(Y\|X)$	8.14 ± 0.08	3.56 ± 0.38	0.51	–	0.60
	mFITEXY $(Y\|X)$	8.18 ± 0.06	3.27 ± 0.21	0.51	$0.22^{+0.10}_{-0.07}$	0.45
	`linmix_err` $(Y\|X)$	8.17 ± 0.06	3.17 ± 0.24	0.51	0.29 ± 0.07	0.56
	BCES $(X\|Y)$	8.14 ± 0.08	3.56 ± 0.25	0.51	–	0.60
	mFITEXY $(X\|Y)$	8.18 ± 0.06	3.51 ± 0.23	0.51	$0.23^{+0.10}_{-0.07}$	0.60
	`linmix_err` $(X\|Y)$	8.17 ± 0.07	3.49 ± 0.26	0.51	0.30 ± 0.07	0.60
	BCES Bisector	8.14 ± 0.08	3.56 ± 0.29	0.51	–	0.60
	mFITEXY Bisector	8.18 ± 0.06	3.39 ± 0.15	0.51	–	0.58
	`linmix_err` Bisector	8.17 ± 0.07	3.33 ± 0.18	0.51	–	0.57
Elliptical (30)	BCES $(Y\|X)$	8.80 ± 0.53	-18.16 ± 53.99	0.76	–	3.02
	mFITEXY $(Y\|X)$	8.90 ± 0.10	4.47 ± 0.88	0.76	$0.29^{+0.14}_{-0.10}$	0.56
	`linmix_err` $(Y\|X)$	8.84 ± 0.12	3.56 ± 1.35	0.76	0.44 ± 0.12	0.59
	BCES $(X\|Y)$	8.80 ± 0.18	8.00 ± 2.55	0.76	–	1.01
	mFITEXY $(X\|Y)$	8.92 ± 0.15	6.85 ± 1.75	0.76	$0.36^{+0.20}_{-0.15}$	0.89
	`linmix_err` $(X\|Y)$	8.89 ± 0.20	6.96 ± 2.49	0.76	0.63 ± 0.30	0.89
	BCES Bisector	8.80 ± 0.11	-0.03 ± 0.10	0.76	–	0.64
	mFITEXY Bisector	8.91 ± 0.13	5.42 ± 0.85	0.76	–	0.73
	`linmix_err` Bisector	8.85 ± 0.16	4.73 ± 1.30	0.76	–	0.67
Lenticular (11)	BCES $(Y\|X)$	7.75 ± 0.58	-11.51 ± 31.78	0.33	–	2.11
	mFITEXY $(Y\|X)$	7.65 ± 0.12	3.78 ± 1.20	0.33	$0.00^{+0.00}_{-0.00}$	0.26
	`linmix_err` $(Y\|X)$			0.33		
	BCES $(X\|Y)$	7.75 ± 0.13	3.54 ± 0.99	0.33	–	0.46
	mFITEXY $(X\|Y)$	7.65 ± 0.12	3.78 ± 1.20	0.33	$0.00^{+0.00}_{-0.00}$	0.49
	`linmix_err` $(X\|Y)$			0.33		
	BCES Bisector	7.75 ± 0.13	-0.09 ± 0.15	0.33	–	0.48
	mFITEXY Bisector	7.65 ± 0.12	3.78 ± 0.85	0.33	–	0.49
	`linmix_err` Bisector			0.33	–	
Spiral (17)	BCES $(Y\|X)$	7.18 ± 0.28	6.78 ± 6.62	0.18	–	1.23
	mFITEXY $(Y\|X)$	7.24 ± 0.13	4.48 ± 0.90	0.18	$0.13^{+0.42}_{-0.13}$	0.52
	`linmix_err` $(Y\|X)$	7.22 ± 0.16	3.57 ± 1.36	0.18	0.39 ± 0.19	0.70
	BCES $(X\|Y)$	7.18 ± 0.23	5.48 ± 1.93	0.18	–	0.99
	mFITEXY $(X\|Y)$	7.24 ± 0.14	4.62 ± 0.96	0.18	$0.13^{+0.43}_{-0.13}$	0.85
	`linmix_err` $(X\|Y)$	7.21 ± 0.21	4.86 ± 1.64	0.18	0.45 ± 0.31	0.89
	BCES Bisector	7.18 ± 0.25	6.06 ± 3.66	0.18	–	1.10
	mFITEXY Bisector	7.24 ± 0.14	4.55 ± 0.66	0.18	–	0.84
	`linmix_err` Bisector	7.22 ± 0.19	4.12 ± 1.07	0.18	–	0.77
Early-type (43)	BCES $(Y\|X)$	8.54 ± 0.10	4.07 ± 0.87	0.64	–	0.65
	mFITEXY $(Y\|X)$	8.58 ± 0.07	3.32 ± 0.34	0.64	$0.24^{+0.10}_{-0.07}$	0.45
	`linmix_err` $(Y\|X)$	8.57 ± 0.08	3.12 ± 0.43	0.64	0.32 ± 0.08	0.53
	BCES $(X\|Y)$	8.54 ± 0.09	3.95 ± 0.55	0.64	–	0.63
	mFITEXY $(X\|Y)$	8.59 ± 0.08	3.88 ± 0.43	0.64	$0.26^{+0.11}_{-0.08}$	0.62
	`linmix_err` $(X\|Y)$	8.59 ± 0.09	3.82 ± 0.50	0.64	0.35 ± 0.10	0.61
	BCES Bisector	8.54 ± 0.10	4.01 ± 0.63	0.64	–	0.64
	mFITEXY Bisector	8.59 ± 0.07	3.58 ± 0.27	0.64	–	0.58
	`linmix_err` Bisector	8.58 ± 0.08	3.44 ± 0.33	0.64	–	0.56

NOTE. — For each subsample, we indicate $\langle \log n_{\rm sph} \rangle$, its average value of spheroid Sérsic index. In the last two columns, we report ϵ, the intrinsic scatter, and Δ, the total rms scatter in the $L_{\rm sph}$ direction. all - mergers - outliers Both the early- and late-type subsamples do not contain the two galaxies classified as S0/Sp and the two galaxies classified as mergers (45+17=66-2-2).

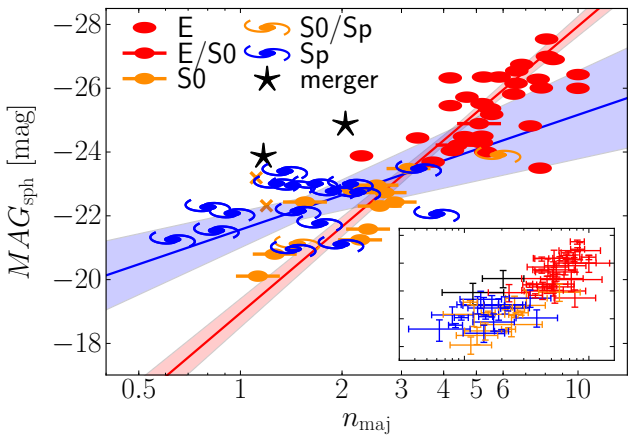
E
E/S0
S0
S0/Sp
Sp
merger
$MAG_{\rm sph}$ [mag]
$n_{\rm maj}$

FIG. 1.—

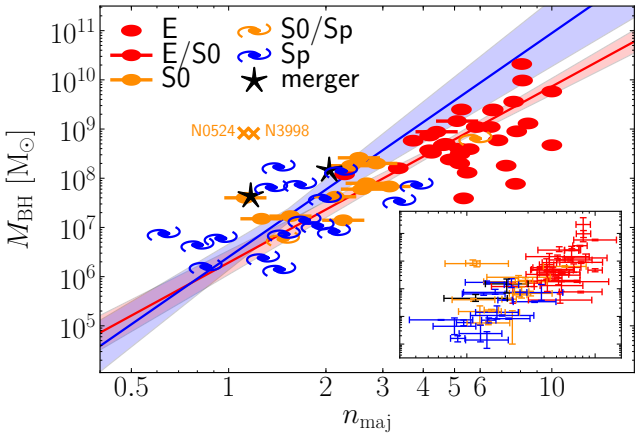
E
E/S0
S0
S0/Sp
Sp
merger
N0524
N3998
$M_{\rm BH}$ [$M_\odot$]
$n_{\rm maj}$

FIG. 2.—